Symmetric Calibration Method of Pendulous Integrating Gyroscopic Accelerometer on Centrifuge

Chuang Sun, Shunqing Ren, Junwei Cao, *Senior Member*, *IEEE*, Ru Huo

***Abstract*—With increasing requirements for the accuracy of Pendulous Integrating Gyroscopic Accelerometer (PIGA), developing effective methods that can accurately calibrate nonlinear error parameters of PIGA is a necessity. In this paper, the symmetric position calibration method is proposed to calibrate the main nonlinear error coefficients of PIGA within integer precession periods on the centrifuge. Firstly, coordinate systems are established, and specific forces, as well as angular velocities of PIGA, are deduced. Then, the complete error calibration model of PIGA, including the high-order error terms, is established. Calibration methods in symmetric positions are proposed, while the closure errors are restrained by the reasonable design of the test time. Moreover, misalignments are suppressed, and installation displacement errors are automatically compensated by the proposed calibration method. Thus, the impact of centrifuge errors on the measurement accuracy of PIGA is effectively suppressed, thereby reducing output uncertainty of PIGA to 10^{-6} rad/s. The simulation results show that the order of calibration uncertainty of PIGA's second-order error parameter is decreased from 10^{-6} to 10^{-7}. Furthermore, the order of calibration uncertainty of other nonlinear error term coefficients is lowered to less than 10^{-6}. Finally, the calibration accuracy of PIGA reaches 1×10^{-7}g/g.**

***Index Terms*—PIGA, nonlinear error term, calibration, error analysis, symmetric position, centrifuge**

I. Introduction

After several decades of extensive research and development, Pendulous Integrating Gyroscopic Accelerometer (PIGA) has become one of the mostwidely employed sensors for Inertial Navigation System(INS). Although the new inertial sensors such as Micro-Electro-Mechanical System (MEMS) sensors and quartz accelerometer have decreased the cost of and are more sensitive in some aspects [1, 2], PIGA will most likely be an irreplaceable sensor in Intercontinental Ballistic Missiles (ICBM) and Submarine Launched Ballistic Missiles (SLBM) systems 30 years from now due to its high precision and strong anti-interference [3].

As a primary technology for improving the performance of linear accelerometers, calibration testing could be roughly classified into several categories, as shown in Fig.1.

Self-Calibration: Self-calibration methods can be used for testing gyro drifts and linear parameters of accelerometers without an external device. Nonlinear errors of accelerometers are calibrated by optimally estimating the navigation errors in rotational inertial navigation systems [4]. By utilizing low precision turntables and filter techniques, the calibration efficiency can be further improved for multi-accelerometers and accelerometer arrays [5-7]. Although the testing cost is significantly decreased by self-calibration methods, the calibration accuracy is generally more than 100ppm as shown in Fig.1, which is significantly low for inertial navigation requirements.

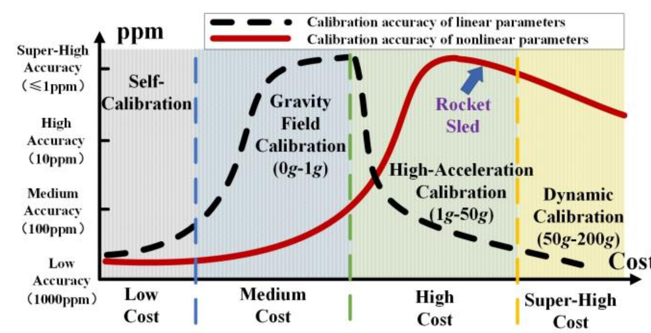

Fig.1. Development of calibration testing of linear accelerometers. The abbreviation ppm means "parts per million".

Gravity Field Calibration: To characterize the bias and scale factor of accelerometers in the gravity field, a precision rotation test is generally employed by utilizing the dividing head and the turntable [8]. The calibration of MEMS accelerometer accuracy can reach 100ppm by using the new six-positions method [9]. Higher costs are driven by the ability to control more attitudes of accelerometers with the need to purchase more advanced precision rotation devices such as the tri-axial turntable [10]. The composite error of accelerometers could be decreased from 100ppm to 10 ppm, while nonlinear errors can also be calibrated in the gravity field [11-14]. However, due to the maximum limit (1 g) that cannot effectively excite nonlinear errors, their calibration accuracy in

This paragraph of the first footnote will contain the date on which you submitted your paper for review.

C. Sun is with the Tsinghua University, Beijing, 100084, China (e-mail: sun489495923@163.com).

J.W. Cao is with the Tsinghua University, Beijing, 100084, China (e-mail: jcao@tsinghua.edu.cn).

R. Huo is with the Beijing University Of Technology, Beijing, 100124, China(e-mail: huoru@bjut.edu.cn)

the gravity field is lower than 100ppm, as shown in Fig.1.

High-Acceleration Calibration: Nonlinear parameters will have a more significant impact on navigation systems. More specifically, the sensors work in an overloaded environment where the input accelerations could be more than 20 g. High-acceleration calibration methods are proposed to calibrate nonlinear error parameters, which can provide 1g-50g input accelerations for accelerometers by utilizing elements such as centrifuge, vibrator, and rocket sled [15]. As shown in Fig.1, the calibration accuracy of nonlinear parameters could be significantly improved from 100 ppm to 10 ppm. Moreover, complex instruments and an overloaded working environment will result in additional interference when calibrating linear parameters. Lastly, it should be mentioned that, the calibration accuracy of linear parameters deteriorates rapidly [16]. Compared with the high cost of rocket sleds and low acceleration output of vibrators [17], centrifuge testing is the most typical calibration equipment for high-precision accelerometers such as PIGA [18]. In contrast to the large-scale centrifuge (radius higher than 2 m) in [19], the disk centrifuge (typical radius of 1 m) is more economical and efficient equipment. With the development of precision test equipment and calibration methods, the calibration accuracy could be less than 10ppm on centrifuge [20, 21]. In addition, by calculating and aligning the main error sources of the disk centrifuge, such as radius errors and misalignment errors, the calibration accuracy could be further enhanced [22,23].

Dynamic Calibration: In essence, the main purpose of rocket sleds is to measure the dynamic performance of accelerometer systems [15]. Researchers tend to pay more attention to characterizing the dynamic performance as opposed to high-precision calibration. Thus, the accuracy of the rocket sled test generally is lower than the accuracy of the precision centrifuge test, as shown in Fig.1. Recently, a new approach is proposed to calibrate the quartz accelerometer on a dynamic centrifuge [24]. However, a new dynamic centrifuge means more complex system and higher costs.

In this paper, to decrease the complexity and costs of calibration tests, new calibration method on a low-cost precision centrifuge is proposed. Since the salient difference between PIGA and other precision accelerometers is the special gyro structure, a more complete error model of PIGA should be deduced and the test process should be optimized. The contributions of this paper are as follows.

1. The complete error calibration model of PIGA is established. The error model not only includes common nonlinear error terms, but also considers the angular velocity quadratic term and mixed quadratic term that is caused by the high rotation velocity of the centrifuge's main axis. In addition, the exact derivation and simulation of closure errors are expressed to clearly illustrate the influence on the accuracy.

2. The symmetric position calibration method is proposed to calibrate the main nonlinear error coefficients of PIGA. This method can suppress the influence of the disk centrifuge errors and closure errors during the test. The main error sources such as misalignments and installation errors could be automatically avoided by the symmetric position test. In addition, the integer periods sampling of PIGA precession can restrain the sampling error and significantly improve the output accuracy of PIGA.

The rest of the paper is organized as follows. In Section II, corresponding coordinate systems are established and precise inputs of PIGA are calculated. The error calibration models are deduced in Section III based on the complete error model of PIGA. In Section IV, the closure errors are deduced and analyzed. The calibration procedure is designed, and the calibration accuracy is evaluated in Section V. The simulations are established and the calibration results are analyzed in Section VI. Finally, the conclusions are given in Section VII.

II. Corresponding Coordinate Systems and Precision Input of PIGA

As shown in Fig. 2, the centrifuge is characterized by three working turntables on the disk, i.e., three PIGA can be simultaneously calibrated. Thus, the test efficiency can be increased when compared to the counter-rotating platform centrifuge in [19]. The nominal working radius of the centrifuge is $R_0 = 0.5$ m. For the angular velocity of the main axis ω, the centrifuge can provide constant centripetal acceleration $R_0\omega^2$ along the radius-sensitive direction.

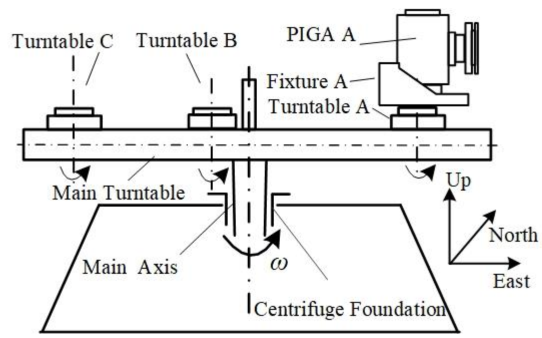

Fig.2. Structure of the disk centrifuge. The centrifuge mainly consists of foundation, main axis, main turntable, and three turntables.

Turntable A and PIGA A are taken as an example. The corresponding coordinate systems are established as follows.

1) Geographic coordinate system o_0-$x_0y_0z_0$, where axes o_0x_0, o_0y_0, and o_0z_0 respectively coincide with local horizontal east, horizontal north, and vertical upward.

2) Centrifuge foundation coordinate system o_1-$x_1y_1z_1$, whose origin o_1 is located on the main axis. The error sources $\Delta\theta_{x0}$ and $\Delta\theta_{y0}$ are perpendicularity with respect to the horizontal plane. Its homogeneous transformation matrix (H-matrix) with respect to o_0-$x_0y_0z_0$ can be expressed as:

$$\boldsymbol{T}_1^0 = \mathrm{Rot}(x_0, \Delta\theta_{x0})\ \mathrm{Rot}(y_0, \Delta\theta_{y0}) = \begin{bmatrix} \boldsymbol{A}_1 & \boldsymbol{0} \\ \boldsymbol{0} & 1 \end{bmatrix}, \quad (1)$$

where Rot represents the rotation of attitude, and $\boldsymbol{A}_1$ is the directional cosine matrix:

$$\boldsymbol{A}_{d1} = \begin{bmatrix} 1 & 0 & \Delta\theta_{y0} \\ 0 & 1 & -\Delta\theta_{x0} \\ -\Delta\theta_{y0} & \Delta\theta_{x0} & 1 \end{bmatrix}.$$

3) Main axis coordinate system o_2-$x_2y_2z_2$, has its origin o_2 that coincides with o_1. The main axis rotates about the axis o_1z_1 with the angular velocity of ω. The main error sources contain the

axial runout $\Delta x_1(\omega t)$ and $\Delta y_1(\omega t)$ as well as, the axial wobble $\phi_x(\omega t)$ and $\phi_y(\omega t)$. These errors can be expressed as:

$$\begin{cases}\Delta x_1(\omega t)=\delta\cos(\omega t+\varphi_0)=\delta_c\cos\omega t-\delta_s\sin\omega t\\ \Delta y_1(\omega t)=\delta\sin(\omega t+\varphi_0)=\delta_s\cos\omega t+\delta_c\sin\omega t\end{cases}, \quad (2)$$

$$\begin{cases}\phi_x(\omega t)=\sum_{n=1}^{\infty}\left(\phi_{xcn}\cos n\omega t+\phi_{xsn}\sin n\omega t\right)\\ \phi_y(\omega t)=\sum_{n=1}^{\infty}\left(\phi_{ycn}\cos n\omega t+\phi_{ysn}\sin n\omega t\right)\end{cases}. \quad (3)$$

Its H-matrix with respect to o_1-$x_1y_1z_1$ can be written as:

$$T_2^1=\mathrm{Rot}(x_1,\phi_x(\omega t))\mathrm{Rot}(y_1,\phi_y(\omega t))\cdot\mathrm{Trans}(\Delta x_1(\omega t),\Delta y_1(\omega t),0)\mathrm{Rot}(z_1,\omega t)=\begin{bmatrix}\boldsymbol{A}_2 & \boldsymbol{D}_2\\ \boldsymbol{0} & 1\end{bmatrix}, \quad (4)$$

where the meaning of matrix $\boldsymbol{A}_2$ is similar to that of A_1, Trans represents the position translation of the origin, and $\boldsymbol{D}_2$ is the translation vector:

$$\boldsymbol{D}_2=\begin{bmatrix}\Delta x_1(\omega t) & \Delta y_1(\omega t) & 0\end{bmatrix}^{\mathrm{T}}.$$

4) Turntable A coordinate system o_3-$x_3y_3z_3$. The nominal radius of the centrifuge is R_0= 0.5 m. The dynamic radius errors can be assumed as negligible since their value is significantly lowered on the disk centrifuge. The main error sources contain perpendicularity parameters $\Delta\lambda_x$ and $\Delta\lambda_y$, axial wobbles $\Delta\theta_{x1}(\theta)$ and $\Delta\theta_{y1}(\theta)$, static radius error ΔR_s, and angular position error $\Delta\theta$. The H-matrix of the coordinate system with respect to o_2-$x_2y_2z_2$ can be expressed as:

$$T_3^2=\mathrm{Trans}(R_0+\Delta R_s,0,0)\mathrm{Rot}(x_2,\Delta\lambda_x+\Delta\theta_{x1}(\theta))\cdot\mathrm{Rot}(y_2,\Delta\lambda_y+\Delta\theta_{y1}(\theta))\mathrm{Rot}(z_2,\theta+\Delta_d)=\begin{bmatrix}\boldsymbol{A}_3 & \boldsymbol{D}_3\\ \boldsymbol{0} & 1\end{bmatrix}. \quad (5)$$

5) Fixture A coordinate system o_4-$x_4y_4z_4$, has its origin o_4 on the turntable rotation axis. The translation displacement is l_1. The main error sources contain the displacement errors Δx_2, Δy_2, and Δz_2. The H-matrix of the coordinate system with respect to o_3-$x_3y_3z_3$ can be expressed as:

$$T_4^3=\mathrm{Trans}(\Delta x_2,\Delta y_2,\Delta z_2+l_1)=\begin{bmatrix}\boldsymbol{A}_4 & \boldsymbol{D}_4\\ \boldsymbol{0} & 1\end{bmatrix}. \quad (6)$$

6) PIGA A coordinate system o_5-$x_5y_5z_5$, has its origin o_5 on the effective center of mass (ECM) of PIGA. The translation displacement along the o_5z_5 axis is l_2. The main error sources contain installation angular errors $\Delta\theta_{x2}$, $\Delta\theta_{y2}$, and $\Delta\theta_{z2}$, as well as installation displacement errors Δx_3, Δy_3, and Δz_3. The H-matrix of the coordinate system with respect to o_4-$x_4y_4z_4$ can be expressed as:

$$T_5^4=\mathrm{Trans}(\Delta x_3,\Delta y_3,\Delta z_3+l_2)\,\mathrm{Rot}(x_4,\Delta\theta_{x3})\cdot\mathrm{Rot}(y_4,\Delta\theta_{y3})\,\mathrm{Rot}(z_4,\Delta\theta_{z3})=\begin{bmatrix}\boldsymbol{A}_5 & \boldsymbol{D}_5\\ \boldsymbol{0} & 1\end{bmatrix}. \quad (7)$$

According to the established coordinate systems, centripetal acceleration components along the o_5-$x_5y_5z_5$ system axes are

$$\begin{bmatrix}a_x & a_y & a_z\end{bmatrix}^{\mathrm{T}}=\left(\boldsymbol{A}_2\boldsymbol{A}_3\boldsymbol{A}_4\boldsymbol{A}_5\right)^{\mathrm{T}}\frac{\mathrm{d}^2\boldsymbol{D}}{\mathrm{d}t^2}, \quad (8)$$

where $\boldsymbol{D}=\boldsymbol{D}_2+\boldsymbol{A}_2\boldsymbol{D}_3+\boldsymbol{A}_2\boldsymbol{A}_3\boldsymbol{D}_4+\boldsymbol{A}_2\boldsymbol{A}_3\boldsymbol{A}_4\boldsymbol{D}_5$.

The acceleration components that react to gravity along the o_5-$x_5y_5z_5$ system axes can be expressed as:

$$\begin{bmatrix}a_{gx} & a_{gy} & a_{gz}\end{bmatrix}^{\mathrm{T}}=\left(\boldsymbol{A}_1\boldsymbol{A}_2\boldsymbol{A}_3\boldsymbol{A}_4\boldsymbol{A}_5\right)^{\mathrm{T}}\begin{bmatrix}0 & 0 & g\end{bmatrix}^{\mathrm{T}}. \quad (9)$$

The Coriolis accelerations along the o_5-$x_5y_5z_5$ system axes are

$$\begin{bmatrix}a_{cx}\\ a_{cy}\\ a_{cz}\end{bmatrix}=2\left(\boldsymbol{A}_1\boldsymbol{A}_2\boldsymbol{A}_3\boldsymbol{A}_4\boldsymbol{A}_5\right)^{\mathrm{T}}\left\{\begin{bmatrix}0\\ \omega_{ie}\cos\lambda\\ \omega_{ie}\sin\lambda\end{bmatrix}\times\begin{bmatrix}-R_0\omega\sin\omega t\\ R_0\omega\cos\omega t\\ 0\end{bmatrix}\right\}, \quad (10)$$

where ω_{ie} is the earth rate, and λ is local latitude.

Total input accelerations along the three reference axes of PIGA are given as follows:

$$\begin{cases}a_i=a_x+a_{gx}+a_{cx}\\ a_o=a_y+a_{gy}+a_{cy}\\ a_p=a_z+a_{gz}+a_{cz}\end{cases}, \quad (11)$$

where a_i, a_p, and a_o are input accelerations along with the reference input axis IA, reference pendulous axis PA, and reference output axis OA of PIGA respectively.

The expression of a_i is calculated as follows:

$$a_i=\varphi_g(\theta)g+\left(R_s\sin\theta-\left(R_0+R_c\right)\cos\theta-\Delta x\right)\omega^2+e(\omega t), \quad (12)$$

where

$$\varphi_g(\theta)=\left(\Delta\lambda_x+\Delta\theta_{x1}(\theta)+0.5\phi_{xc1}+0.5\phi_{ys1}\right)\sin\theta-\left(\Delta\lambda_y+\Delta\theta_{y1}(\theta)+0.5\phi_{yc1}-0.5\phi_{xs1}\right)\cos\theta-\Delta\theta_{y2},$$

$$R_c=\left(l_1+l_2\right)\left(\Delta\lambda_y+\Delta\theta_{y1}(\theta)+0.5\phi_{yc1}-0.5\phi_{xs1}\right)+\Delta R_s+2\frac{\omega_{ie}}{\omega}R_0\sin\lambda,$$

$$R_s=\Delta\theta_{z2}R_0+\left(l_1+l_2\right)\left(\Delta\lambda_x+\Delta\theta_{x1}(\theta)+0.5\phi_{ys1}+0.5\phi_{xc1}\right),$$

$$\Delta x=\Delta x_2+\Delta x_3+l_2\Delta\theta_{y2},$$

$$e(\omega t)=\sum_{n=1}^{\infty}\left(e_{cn}\cos n\omega t+e_{sn}\sin n\omega t\right).$$

In Eq. (12), e_{cn} and e_{sn} are harmonic error parameters whose expressions will be given in Section IV. Input acceleration errors of PIGA can be summarized in several components: the gravity errors are caused by misalignment $\varphi_g(\theta)$, the centripetal acceleration errors are caused by radius errors R_c and R_s, the constant centripetal acceleration errors are caused by the installation decentration Δx, and the harmonic acceleration errors are caused by the axial runout and axial wobble.

The angular velocity also significantly affects the accuracy of PIGA. Thus, angular velocities along the three reference axes of PIGA need to be deduced

$$\begin{bmatrix}\omega_i & \omega_o & \omega_p\end{bmatrix}^{\mathrm{T}}=\left(\boldsymbol{A}_1\boldsymbol{A}_2\boldsymbol{A}_3\boldsymbol{A}_4\boldsymbol{A}_5\right)^{\mathrm{T}}\begin{bmatrix}0 & \omega_{ie}\cos\lambda & \omega_{ie}\sin\lambda\end{bmatrix}^{\mathrm{T}}+\left(\boldsymbol{A}_3\boldsymbol{A}_4\boldsymbol{A}_5\right)^{\mathrm{T}}\begin{bmatrix}0 & 0 & \omega\end{bmatrix}^{\mathrm{T}}, \quad (13)$$

where ω_i can be expressed as:

$$\begin{aligned}\omega_i = {} & \omega_{ie}\cos\lambda\sin(\omega t+\theta)+\left(\Delta\lambda_x+\Delta\theta_{x1}(\theta)\right)\omega\sin\theta \\ & -\left(\Delta\lambda_y+\Delta\theta_{y1}(\theta)\right)\omega\cos\theta-\Delta\theta_{y2}\omega\end{aligned} \quad . \quad (14)$$

In Eq. (14), the measurement error of PIGA may be higher than 4.46×10^{-3} m/s^2 without compensation when the ω is 10 rad/s and $\Delta\theta_{y2}$ is 5″. Thus, the error sources of precision centrifuges should be monitored and compensated, while the experimental scheme should be optimized.

III. Error Calibration Model

In Section III, the complete error model for the disk centrifuge testing of PIGA is proposed. The model includes bias, scale factor, second-order term, cross-quadratic term, odd-quadratic term, third-order term, angular velocity quadratic term, and a mixed quadratic term. When the total number of the output pulse of PIGA P_A precession is 16384 per period(2πrad) and the test time is T_m, the average precession angular rate of PIGA $\bar{\dot{\alpha}}$ is obtained as:

$$\begin{aligned}\bar{\dot{\alpha}} = {} & \frac{2\pi P_A}{16384T_m}=\frac{1}{T_m}\int_0^{T_m}[k_0+k_z a_i+k_{zz}a_i^2+k_2'(a_p^2+a_o^2) \\ & +k_{oq}a_i\left|a_i\right|+k_\omega(a_o\omega_o+a_p\omega_p)a_i+k_3a_i^3 \\ & -(1-\delta_z a_i)\omega_i+\Omega_2'(\omega_o^2+\omega_p^2)+\varepsilon]\mathrm{d}t\end{aligned} \quad , (15)$$

where k_0 is bias(rad·s^{-1}), k_z is the scale factor ((rad·s^{-1})/g), k_{zz} is the second-order error coefficient ((rad·s^{-1})/g^2), k_2' is the cross-quadratic error coefficient((rad·s^{-1})/g^2) , k_{oq} is the odd-quadratic error coefficient((rad·s^{-1})/g^2), k_ω is the cross-over error coefficient(g^{-2}), k_3 is the third-order error coefficient((rad·s^{-1})/g^3), δ_z is the couple error coefficient(g^{-1}), Ω_2' is the second-order angular error coefficient (rad·s^{-1})$^{-1}$, and ε is the random error(rad·s^{-1}).

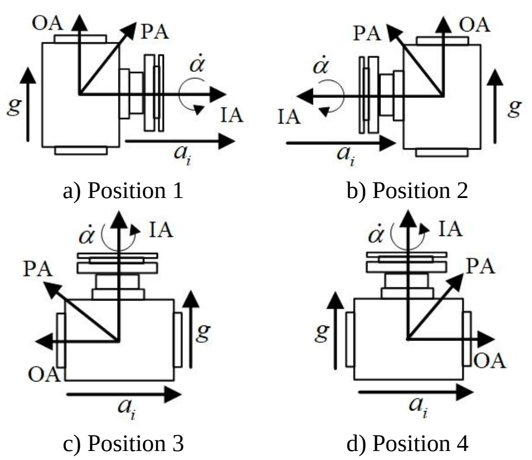

Fig.3. Installation positions of PIGA on the centrifuge.

Symmetry positions of PIGA are shown in Fig.3. In position 1, OA axis is vertical, IA and PA axes are horizontal, and θ=0 . The average precession angular velocity of PIGA $\bar{\dot{\alpha}}_{aj}$ can be calculated according to Eqs. (12), (13), and (15):

$$\begin{aligned}\bar{\dot{\alpha}}_{aj}^{+} = {} & k_0+k_z\varphi_g(0)g+k_2'g^2 \\ & +\left(\Delta\theta_{y2}+\Delta\lambda_y+\Delta\theta_{y1}(0)\right)\omega_j \\ & -\left(k_z\Delta x-\Omega_2'+k_z\left(R_0+R_c+2k_{zz}\varphi_g(0)R_0\right)\right)\omega_j^2 \\ & +k_{zz}R_0^2\omega_j^4-k_{oq}R_0^2\omega_j^4-k_3R_0^3\omega_j^6+\Delta e_{aj}^{+}+\varepsilon_{aj}^{+}\end{aligned} \quad , \quad (16)$$

where ω_j $(j=1,2,\cdots\cdots,m)$ are the rotation angular velocities of the main axis and Δe_{aj}^{+} is the closure error in position 1.

The output accuracy is improved, while the couple and cross-over errors are restrained by counting the output pulse within integral precession periods. Let the number of the rotation period of the main axis be N and the rotation time be T_N. Since $T_m\neq T_N$, the harmonic error parameters in $e(\omega t)$ cannot be directly ignored. The Δe can be expressed as:

$$\begin{aligned}\Delta e & =\int_{T_N}^{T_m}e(\omega t)\mathrm{d}t \\ & =\frac{k_z}{T_m\omega}\sum_{n=1}^{\infty}\left(e_{sn}\left(\sin n\omega T_m-\sin n\omega T_N\right)+e_{cn}\left(\cos n\omega T_m-\cos n\omega T_N\right)\right)\end{aligned} \quad . (17)$$

The average precession angular velocity of PIGA $\bar{\dot{\alpha}}_{aj}$ in position 2 can be calculated as follws:

$$\begin{aligned}\bar{\dot{\alpha}}_{aj}^{-} = {} & k_0+k_z\varphi_g(0)g+k_2'g^2 \\ & +\left(\Delta\theta_{y2}-\Delta\lambda_y-\Delta\theta_{y1}(\pi)\right)\omega_j \\ & -\left(\left(k_z\Delta x-\Omega_2'\right)-k_z\left(R_0+\Delta R_c+2k_{zz}\varphi_g(\pi)R_0\right)\right)\omega_j^2 \\ & +k_{zz}R_0^2\omega_j^4+k_{oq}R_0^2\omega_j^4+k_3R_0^3\omega_j^6+\Delta e_{aj}^{-}+\varepsilon_{aj}^{-}\end{aligned} \quad , \quad (18)$$

where Δe_{aj}^{-} is the closure error in position 2.

To further improve the calibration accuracy, the symmetric calibration method for calibrating the nonlinear error parameters of PIGA is proposed. By combining Eqs. (16) and (17), the calibration matrix is obtained:

$$\begin{bmatrix}\dfrac{\left(\bar{\dot{\alpha}}_{a1}^{+}+\bar{\dot{\alpha}}_{a1}^{-}\right)}{2}\\ \vdots \\ \dfrac{\left(\bar{\dot{\alpha}}_{am}^{+}+\bar{\dot{\alpha}}_{am}^{-}\right)}{2}\end{bmatrix}=\boldsymbol{A}_a\begin{bmatrix}k_0+0.5k_z\left(\varphi_g(\pi)-\varphi_g(0)\right)g+k_2'g^2\\ \Delta\theta_{y2}+0.5\Delta\theta_{y1}(0)-0.5\Delta\theta_{y1}(\pi)\\ k_z\Delta x-\Omega_2'+k_zR_0\left(k_{zz}\varphi_g(0)-\varphi_g(\pi)\right)\\ k_{zz}\end{bmatrix}+\boldsymbol{e}^{+} \quad (19)$$

$$\begin{bmatrix}\dfrac{\left(\bar{\dot{\alpha}}_{a1}^{+}-\bar{\dot{\alpha}}_{a1}^{-}\right)}{2}\\ \vdots \\ \dfrac{\left(\bar{\dot{\alpha}}_{am}^{+}-\bar{\dot{\alpha}}_{am}^{-}\right)}{2}\end{bmatrix}=\boldsymbol{A}_a\begin{bmatrix}-0.5k_z\left(\varphi_g(0)+\varphi_g(\pi)\right)g\\ \Delta\lambda_y+0.5\Delta\theta_{y1}(0)+0.5\Delta\theta_{y1}(\pi)\\ k_z\left(R_0+R_c+k_{zz}\left(\varphi_g(0)+\varphi_g(\pi)\right)R_0\right)\\ -k_{oq}\\ -k_3\end{bmatrix}+\boldsymbol{e}^{-} \quad (20)$$

where $\boldsymbol{A}_a=\begin{bmatrix}1 & \omega_1 & -\omega_1^2 & R_0^2\omega_1^4\\ \vdots & \vdots & \vdots & \vdots\\ 1 & \omega_m & -\omega_m^2 & R_0^2\omega_m^4\end{bmatrix}$.

It should be noted that the calibration test in position 1 and position 2 can greatly simplify the structure of the error calibration model and automatically restrain the influence of cross-over error on the calibration. In order to identify the nonlinear error parameters of PIGA by utilizing the Least Square (LS) algorithm without the influence from the closure errors matrix $\boldsymbol{e}^{+}$ and $\boldsymbol{e}^{-}$ in Eqs. (18) and (19), the T_m and T_N should be first optimally designed. Then, the proposed calibration method can accurately identify k_{zz}, k_{oq}, and k_3.

However, the test in positions 1 and 2 cannot provide sufficient input acceleration to excite the PA axis and OA axis of PIGA. Therefore, to calibrate the cross-quadratic error parameter, it is necessary to design other symmetrical installation positions. As shown in Fig.4 (c) and (d), the average precession angular velocity of PIGA in positions 3 and 4 can be respectively calculated as follows:

$$\begin{aligned}\bar{\dot{\alpha}}_{gj}^{+}=&k_0+k_z\left(\Delta\lambda_x+\Delta\theta_{x1}(0)+\Delta\theta_{x2}\right)g+\left(k_{zz}+k_{oq}\right)g^2-\omega_j\\&-k_z\left(\Delta\lambda_y+\Delta\theta_{y1}(0)+\Delta\theta_{y2}+0.5\phi_{yc1}-0.5\phi_{xs1}\right)R_0\omega_j^2\\&+k_2'\left(1+2\Delta x/R_0\right)R_0^2\omega_j^4+k_3g^3-\omega_{ie}\sin\lambda+\Delta e_{gj}^{+}+\varepsilon_{gj}^{+}\end{aligned}\quad,\ (21)$$

$$\begin{aligned}\bar{\dot{\alpha}}_{gj}^{-}=&k_0+k_z\left(\Delta\lambda_x+\Delta\theta_{x1}(\pi)+\Delta\theta_{x2}\right)g+\left(k_{zz}+k_{oq}\right)g^2-\omega_j\\&-k_z\left(\Delta\lambda_y+\Delta\theta_{y1}(\pi)-\Delta\theta_{y2}+0.5\phi_{yc1}-0.5\phi_{xs1}\right)R_0\omega_j^2\\&+k_2'\left(1+2\Delta x/R_0\right)R_0^2\omega_j^4+k_3g^3-\omega_{ie}\sin\lambda+\Delta e_{gj}^{-}+\varepsilon_{gj}^{-}\end{aligned}\quad,\ (22)$$

where Δe_{gj}^{+} and Δe_{gj}^{-} are closure errors in positions 3 and 4, respectively.

Since some error terms are irrelevant to ω_j in Eqs. (21) and (22), the static test should be designed to eliminate some influence of gravity components. When the angular velocity of the main axis is 0 rad/s and closure errors are not accounted for, the average precession angular velocity of PIGA in position3 3 and 4 can be expressed as:

$$\begin{aligned}\bar{\dot{\alpha}}_{g0}^{+}=&k_0+k_z\left(\Delta\lambda_x+\Delta\theta_{x1}(0)+\Delta\theta_{x2}\right)g\\&+\left(k_{zz}+k_{oq}\right)g^2-\omega_{ie}\sin\lambda+k_3g^3+\varepsilon_{g0}^{+}\end{aligned},\quad (23)$$

$$\begin{aligned}\bar{\dot{\alpha}}_{g0}^{-}=&k_0+k_z\left(\Delta\lambda_x+\Delta\theta_{x1}(\pi)+\Delta\theta_{x2}\right)g\\&+\left(k_{zz}+k_{oq}\right)g^2+\omega_{ie}\sin\lambda+k_3g^3+\varepsilon_{g0}^{-}\end{aligned}.\quad (24)$$

Thus, without considering the closure errors, the error parameters of these calibration models can be identified.

$$\hat{\boldsymbol{k}}_g=\left(\boldsymbol{\Phi}_g^{\mathrm{T}}\boldsymbol{\Phi}_g\right)^{-1}\boldsymbol{\Phi}_g^{\mathrm{T}}\begin{bmatrix}0.5\left(\bar{\dot{\alpha}}_{g1}^{+}+\bar{\dot{\alpha}}_{g1}^{-}-\bar{\dot{\alpha}}_{g0}^{+}-\bar{\dot{\alpha}}_{g0}^{-}\right)+\omega_1\\\vdots\\0.5\left(\bar{\dot{\alpha}}_{gm}^{+}+\bar{\dot{\alpha}}_{gm}^{-}-\bar{\dot{\alpha}}_{g0}^{+}-\bar{\dot{\alpha}}_{g0}^{-}\right)+\omega_m\end{bmatrix},(25)$$

where

$$\hat{\boldsymbol{k}}_g=\begin{bmatrix}k_z\left(\Delta\lambda_y+0.5\Delta\theta_{y1}(0)+0.5\Delta\theta_{y1}(\pi)+0.5\phi_{yc1}-0.5\phi_{xs1}\right)\\k_2'\end{bmatrix},$$

$$\boldsymbol{\Phi}_g=\begin{bmatrix}-R_0\omega_1^2 & R_0^2\omega_1^4\\\vdots & \vdots\\-R_0\omega_m^2 & R_0^2\omega_m^4\end{bmatrix}.$$

Eq. (25) illustrates that the symmetric calibration model can automatically avoid installation errors and accurately identify the error parameter k_2'. In addition, the harmonic component of the errors in the error calibration model of PIGA could be decreased by integral period rotation of the centrifuge. Thus, the measurement accuracy of PIGA can be further improved.

IV. Closure Error Analysis and Suppression

According to the calibration models in Section III, closure errors are the main error source in the models. Thus, in order to eliminate or reduce the influence on the calibration accuracy of PIGA, it is necessary to analyze the closure errors and to design an optimal test scheme.

Let the PIGA be installed in position 1, the original angle of the main axis be $\phi_N=\omega T_N$, and the ending angle of the main axis be $\phi_m=\omega T_m$. Only the first-order, second-order, and third-order harmonic terms are considered in the closure errors. The parameter Δe_a^{+} can be expressed as:

$$\begin{aligned}\Delta e_a^{+}=&\left(es_1\left(\sin\phi_m-\sin\phi_N\right)+ec_1\left(\cos\phi_m-\cos\phi_N\right)\right.\\&-0.25es_2\left(\sin2\phi_m-\sin2\phi_N\right)-0.25ec_2\left(\cos2\phi_m-\cos2\phi_N\right)\\&\left.-es_3\left(\sin3\phi_m-\sin3\phi_N\right)/6-ec_3\left(\cos3\phi_m-\cos3\phi_N\right)/6\right)/T_m\omega\end{aligned}\quad,(26)$$

where

$$es_1=0.5\left(\omega^2\left(l_1+l_2\right)k_z+k_zg-\omega\right)\left(\phi_{xs2}-\phi_{yc2}\right)-4k_z\delta_c\omega^2-\Delta\theta_{y0},$$

$$\begin{aligned}ec_1=&0.5\left(\omega^2\left(l_1+l_2\right)k_z+k_zg-\omega\right)\left(\phi_{ys2}+\phi_{xc2}\right)\\&-4k_z\delta_s\omega^2+\omega_{ie}\omega\cos\lambda-\Delta\theta_{x0}\end{aligned},$$

$$es_2=\left(\omega^2\left(l_1+l_2\right)k_z+k_zg-\omega\right)\left(\phi_{yc1}+\phi_{xs1}\right),$$

$$ec_2=\left(\omega^2\left(l_1+l_2\right)k_z+k_zg-\omega\right)\left(\phi_{xc1}-\phi_{ys1}\right),$$

$$es_3=\left(\omega^2\left(l_1+l_2\right)k_z+k_zg-\omega\right)\left(\phi_{yc2}+\phi_{xs2}\right),$$

$$ec_3=\left(\omega^2\left(l_1+l_2\right)k_z+k_zg-\omega\right)\left(\phi_{xc2}-\phi_{ys2}\right).$$

Eq. (26) shows that the first-order harmonic components of the closure error are mainly caused by the runout of the main axis. Moreover, the high-order harmonic components of the closure error are mainly caused by axial wobble on the centrifuge. The simulation is given in Fig.4.

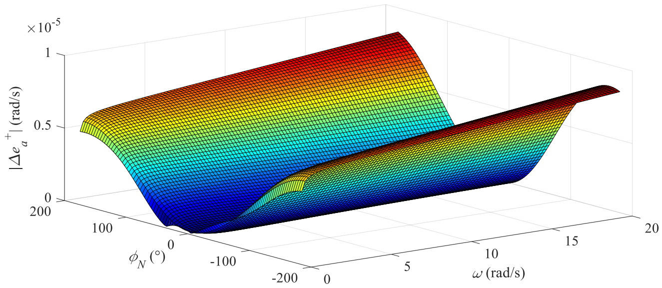

Fig. 4. Simulation results of closure error for the test time 20 s in position 1.

According to Fig.5, Δe_a^{+} is significantly increase with ϕ_N and ω. The parameter $\left|\Delta e_a^{+}\right|$ could be larger than 5×10^{-6}rad/s when the angular velocity ω is higher than 15rad/s, i.e., the measurement error of PIGA could be larger than 1.5×10^{-5} g. The closure error must be restrained during the test when the requirement of calibration accuracy is 1×10^{-6}g/ g.

If the PIGA is installed in position 3, the expression of Δe_g^{+}

is as follows:

$$\begin{aligned}\Delta e_g^{\ +} = k_z R_0 (& e_{sg1}(\sin\phi_m - \sin\phi_N) + e_{cg1}(\cos\phi_m - \cos\phi_N) \\ & + e_{sg2}(\sin 2\phi_m - \sin 2\phi_N) + e_{cg2}(\cos 2\phi_m - \cos 2\phi_N) \\ & + e_{sg3}(\sin 2\phi_m - \sin 2\phi_N) + e_{cg3}(\cos 2\phi_m - \cos 2\phi_N)) / T_{mg}\end{aligned} \quad ,(26)$$

where

$$e_{sg1} = -\Delta\theta_{y0}\omega - 0.5\phi_{yc2}\omega + 0.5\phi_{xs2}\omega ,$$

$$e_{cg1} = -\Delta\theta_{x0}\omega - 2\omega_{ie}\cos\lambda + 0.5\phi_{ys2}\omega + 0.5\phi_{xc2}\omega ,$$

$$e_{sg2} = -0.25\left(\phi_{yc1}\omega + \phi_{xs1}\omega\right) ,$$

$$e_{cg2} = 0.25\left(\phi_{ys1}\omega - \phi_{xc1}\omega\right) ,$$

$$e_{sg3} = -\left(\phi_{yc2}\omega + \phi_{xs2}\omega\right)/6 ,$$

$$e_{cg3} = \left(\phi_{ys2}\omega - \phi_{xc2}\omega\right)/6 .$$

The harmonic structure of the closure error $\Delta e_g^{\ +}$ is relatively simpler in position 3 as opposed to $\Delta e_a^{\ +}$ in position 1. The simulation of $\Delta e_g^{\ +}$ is given in Fig.5. It should be noted that the maximum value of $\left|\Delta e_g^{\ +}\right|$ is higher than 2×10^{-6}rad/s, and that the angular velocity ω has a stronger influence on $\Delta e_g^{\ +}$ due to the IA axis of PIGA being parallel to the main axis in position 3.

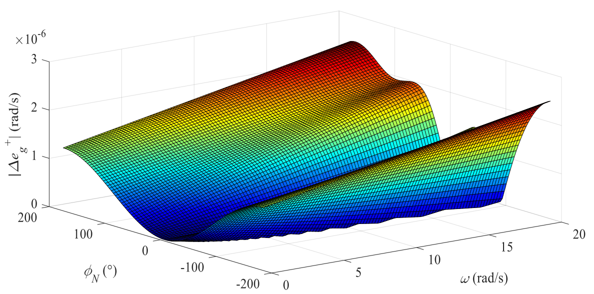

Fig. 5. Simulation results of closure error for the test time 100 s in position 3

According to the simulation results of the closure errors, the number of precession period of PIGA P_N and rotation period of the main axis P_m must be reasonably designed to ensure that the value of T_m and T_N are relatively similar. Let $k_0 + k_z\Delta\varphi_g(0)g = -5\times10^{-4}$rad/s , $\Delta x = 2\times10^{-4}$m , and ω=10rad/s. The simulations of $(\phi_m - \phi_N)$ and $\left|\Delta e_a^{\ +}\right|$ are given in Fig.6.

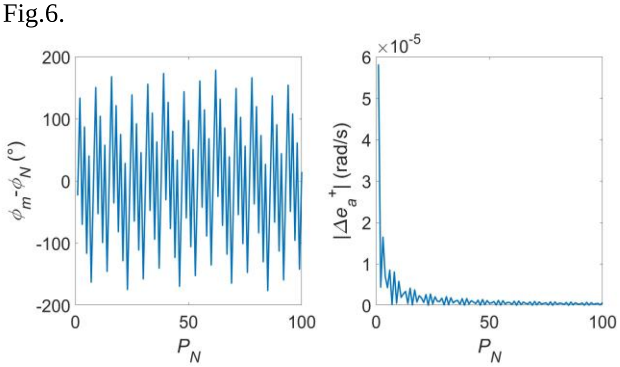

Fig.6. Simulation results of $(\phi_m - \phi_N)$ and $\left|\Delta e_a^{\ +}\right|$

In Fig.6, the change in the value of $(\phi_m - \phi_N)$ is cyclic, while the variation trend in the value of $\left|\Delta e_a^{\ +}\right|$ decreases from 5×10^{-5} rad/s to 4.19×10−10rad/s (P_N=23) with an increase in the number of precession periods of PIGA. Thus, the measurement acceleration errors caused by the closure errors can be suppressed to 1×10^{-8}g.

V. Calibration Procedure and Accuracy Evaluation

The symmetric calibration method within PIGA integer precession periods is designed to the established error calibration models in Section III and the analysis of closure errors in Section IV (Fig.7).

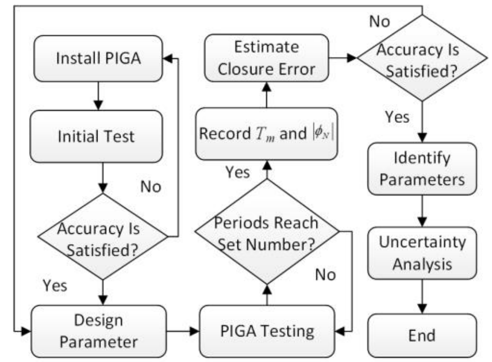

Fig. 7. Flowchart of PIGA test on the disk centrifuge

The calibration test procedure is as follows.

1) The PIGA should be installed on the fixture correctly.

2) The initial test includes the alignment test, working radius measurement, and position adjustment. The detailed test process is given in [19] and [24].

3) When the initial test results satisfy the accuracy requirement of the calibration test, the corresponding test parameters should be calculated and designed. These parameters include but are not limited to, the number of precession periods of PIGA, the angular velocity of the main axis, and the initial angular position of the main axis.

4) Once the instruments are running stably, the test can be commenced. The number of the precession periods of PIGA, the test time, and the angular position of the main axis are recorded. In addition, the running parameters of the centrifuge should also be monitored.

5) When the number of the precession periods of PIGA reaches the set value, values of T_m and ϕ_N are recorded. Then, the closure errors can be estimated.

6) If the estimation results satisfy the accuracy requirement, the following test step can be continued. If not, the parameters should be redesigned.

7) By utilizing the LS algorithm, nonlinear error parameters of PIGA can be identified by the proposed calibration methods.

8) Finally, the uncertainty analysis should be conducted to illustrate the accuracy of the calibration methods.

In order to analyze the validity and feasibility of the proposed calibration method, the accuracy should be evaluated before the test. The calibration test of PIGA in position 1 is taken as an example. Calibration uncertainties of the parameters can be calculated as:

$$\begin{cases} \sigma_{k_{zz}} = \sqrt{\left(a_{41}\sigma_{a1}{}^{+}\right)^2 + \left(a_{42}\sigma_{a2}{}^{+}\right)^2 + \cdots\cdots + \left(a_{4n}\sigma_{an}{}^{+}\right)^2} \\ \quad = 1.8\times10^{-7}\ \text{rad/s/g}^2 \\ \sigma_{k_{oq}} = \sqrt{\left(a_{41}\sigma_{a1}{}^{-}\right)^2 + \left(a_{42}\sigma_{a2}{}^{-}\right)^2 + \cdots\cdots + \left(a_{4n}\sigma_{an}{}^{-}\right)^2} \\ \quad = 5.4\times10^{-6}\ \text{rad/s/g}^2 \\ \sigma_{k_3} = \sqrt{\left(a_{51}\sigma_{a1}{}^{+}\right)^2 + \left(a_{52}\sigma_{a2}{}^{+}\right)^2 + \cdots\cdots + \left(a_{5n}\sigma_{an}{}^{+}\right)^2} \\ \quad = 2.1\times10^{-7}\ \text{rad/s/g}^3 \end{cases}, \quad (27)$$

where a_{ij} ($i=1,2,\cdots\cdots,n$, and $j=1,2,3,4$) represent elements in the matrix $\left(\left(\boldsymbol{A}_a\right)^{\mathrm{T}}\boldsymbol{A}_a\right)^{-1}\left(\boldsymbol{A}_a\right)^{\mathrm{T}}$. $\sigma_{ai}{}^{+}$ and $\sigma_{ai}{}^{-}$ are the output accuracies of PIGA that are set to 1×10^{-6}rad/s. The calculation results indicate that the proposed calibration method can accurately calibrate the nonlinear errors of PIGA. The calibration uncertainty of k_{zz} is lower than 2×10^{-7} rad/s/g, which is significantly lower than the uncertainty of k_{oq}. By analyzing the characteristics of the calibration model and LS algorithm, it is found that the proposed symmetry calibration method sacrifices the calibration accuracy of k_{oq} and k_3 in order to improve the calibration accuracy of k_{zz}.

According to Eq. (25), the measurement uncertainty in position3 3 and 4 can be calculated as follows:

$$\sigma_{Ygj} = \sqrt{\begin{array}{l} \left(\dfrac{\partial Y_{gj}}{\partial \bar{\dot{\alpha}}_{gj}{}^{+}}\sigma_{gj}{}^{+}\right)^2 + \left(\dfrac{\partial Y_{gj}}{\partial \bar{\dot{\alpha}}_{gj}{}^{-}}\sigma_{gj}{}^{-}\right)^2 \\ + \left(\dfrac{\partial Y_{gj}}{\partial \bar{\dot{\alpha}}_{g0}{}^{+}}\sigma_{g0}{}^{+}\right)^2 + \left(\dfrac{\partial Y_{gj}}{\partial \bar{\dot{\alpha}}_{g0}{}^{-}}\sigma_{g0}{}^{-}\right)^2 + \left(\dfrac{\partial Y_{gj}}{\partial \omega_j}\sigma_{\omega}\right)^2 \end{array}}, \quad (28)$$

where $Y_{gj} = 0.5\left(\bar{\dot{\alpha}}_{gj}{}^{+} + \bar{\dot{\alpha}}_{gj}{}^{-} - \bar{\dot{\alpha}}_{g0}{}^{+} + \bar{\dot{\alpha}}_{g0}{}^{-}\right) + \omega_j$. $\sigma_{gj}{}^{+}$, $\sigma_{gj}{}^{-}$, $\sigma_{g0}{}^{+}$, and $\sigma_{g0}{}^{-}$ are the output accuracies of PIGA in positions 3 and 4. σ_{ω} is the angular velocity accuracy of the main axis that should be lower than 3×10^{-6}rad/s.

The calibration uncertainties of k_2' can be estimated as:

$$\sigma_{k_2'} = \sqrt{\left(g_{31}\sigma_{Yg1}\right)^2 + \left(g_{32}\sigma_{Yg2}\right)^2 + \cdots\cdots + \left(g_{3m}\sigma_{Ygm}\right)^2} \ , \quad = 6.8\times10^{-7}\ \text{rad/s/g}^2 \quad (29)$$

where g_{ij}($i=1,2,\cdots\cdots,m$, and $j=1,2,3$) represent elements in the matrix $\left(\boldsymbol{\Phi}_g{}^{\mathrm{T}}\boldsymbol{\Phi}_g\right)^{-1}\boldsymbol{\Phi}_g{}^{\mathrm{T}}$.

The evaluation results in Eqs. (27) and (29) show that the magnitude of calibration uncertainty of k_{zz}, k_2' , and k_3 are all lower than 1×10^{-6}. Thus, the proposed method can accurately calibrate the main nonlinear error parameters of PIGA.

Generally, the calibration accuracy r_a (g/g) should also be calculated to evaluate the effectiveness of the calibration result.

$$r_a = \left|r_i / a_{\text{nominal}}(i)\right| \quad (30)$$

where r_i is the residual error and $a_{\text{nominal}(i)}$ is the input nominal acceleration.

VI. Simulation Results

The simulation environment is constructed in this section to verify the availability of the symmetric calibration method. Simulation values of the main parameters of PIGA and the centrifuge are given in Table I.

TABLE I
SET VALUES OF SIMULATION PARAMETERS

Parameters	Value	Parameters	Value
k_0	4×10^{-4}rad/s	Ω_2'	5×10^{-7}(rad/s)$^{-1}$
k_z	0.55rad/s/g	k_ω	5×10^{-10}g^{-2}
k_3	8×10^{-7}rad/s/g^3	$\Delta\lambda_x$, $\Delta\lambda_y$	5×10^{-5}rad
k_{zz}	5×10^{-6}rad/s/g^2	$\Delta\theta_{x2}$, $\Delta\theta_{y2}$, $\Delta\theta_{z2}$	5×10^{-5} rad
k_{oq}	3×10^{-6}rad/s/g^2	$\Delta\theta$	2.5×10^{-6}rad
k_2'	5×10^{-6}rad/s/g^2		

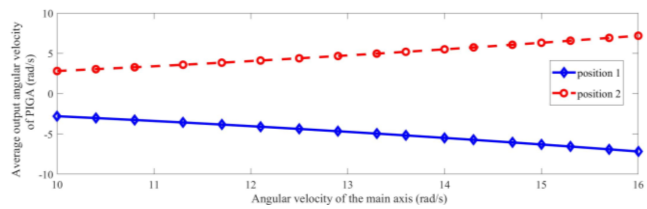

a) Average output angular velocity of PIGA.

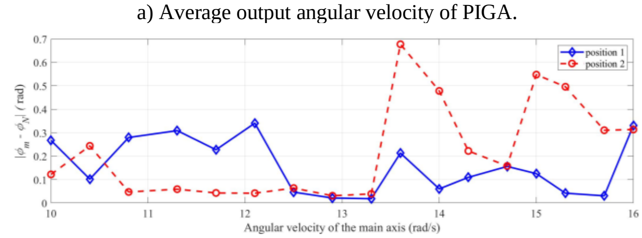

b) The angle of the closure error

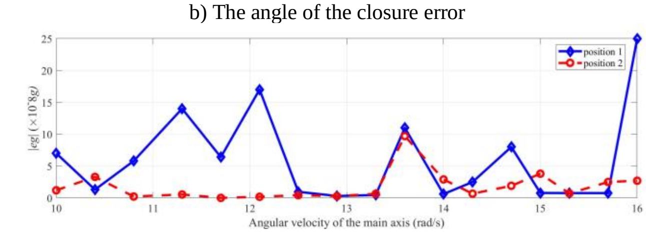

c)The error acceleration components caused by closure errors.

Fig.8. Simulation results in position 1 and 2.

When the angular velocity of the main axis is set from 10 rad to 16 rad, the number of the precession periods of PIGA in positions 1 and 2 can be estimated as shown in Table II.

TABLE II
THE PRECESSION PERIODS OF PIGA IN POSITION 1 AND 2

ω (rad/s)	P_N		ω(rad/s)	P_N	
	Position1	Positio2		Positio1	Positio2
10	30	23	13.6	103	95
10.4	28	28	14	97	138
10.8	53	30	14.3	134	140
11.3	32	26	14.7	134	141
11.7	42	43	15	154	146
12.1	38	37	15.3	179	183
12.5	81	81	15.7	137	155
12.9	89	93	16	136	171
13.3	97	94			

The simulation results of PIGA in positions 1 and 2 are given in Fig.8, where $|eg|$ is the error acceleration components of PIGA caused by the closure errors. In Fig.8.b), the values of

TABLE III
SIMULATION DESIGN OF THE PRECESSION PERIODS OF PIGA

Nonlinear Error Parameter	Symmetry Calibration Method		Symmetry Calibration without Parameter Optimization		Revised Calibration Method [24]	
	Calibration Result	Calibration Uncertainty	Calibration Result	Calibration Uncertainty	Calibration Result	Calibration Uncertainty
k_{zz} (rad/s/g^2)	5.02×10^{-6}	1.01×10^{-7}	5.38×10^{-6}	4.10×10^{-6}	6.25×10^{-6}	2.12×10^{-6}
k_3 (rad/s/g^3)	8.85×10^{-7}	1.00×10^{-7}	8.85×10^{-7}	1.23×10^{-7}	7.49×10^{-7}	4.80×10^{-8}
k_{oq} (rad/s/g^2)	3.16×10^{-7}	4.10×10^{-6}	3.17×10^{-7}	5.45×10^{-6}	5.85×10^{-6}	2.12×10^{-6}

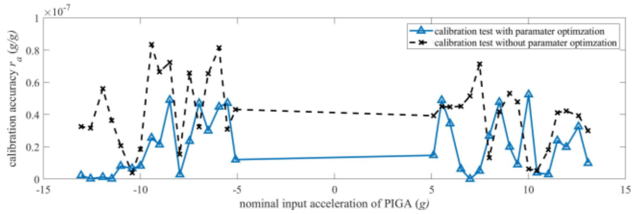

Fig.9. Calibration accuracy in position 1 and 2.

$|\phi_m-\phi_N|$ are all lower than 0.7rad when the optimal parameter is designed. Then, the estimation results of $|eg|$ are all lower than 2.5×10^{-7}g as shown in Fig.8.c). Thus, the closure errors in the calibration models can be ignored.

The identification results of the main nonlinear error parameters of PIGA are given in Table III. Compared with the calibration test without designing the optimal parameter, the proposed calibration process can significantly improve the calibration accuracy. Compared with a revised calibration method in [24], the proposed symmetric calibration method can further improve the calibration accuracy of the second-order error coefficient k_{zz}, which is the primary nonlinear error parameter of PIGA. The calibration uncertainty of k_{zz} is decreased from 2.12×10^{-6} rad/s/g^2 to 1.01×10^{-7} rad/s/g^2. However, the calibration uncertainty of k_{oq} is increased from 2.12×10^{-6} rad/s/g^2 to 5.45×10^{-6} rad/s/g^2. This is also observed for the calibration uncertainty of k_3.

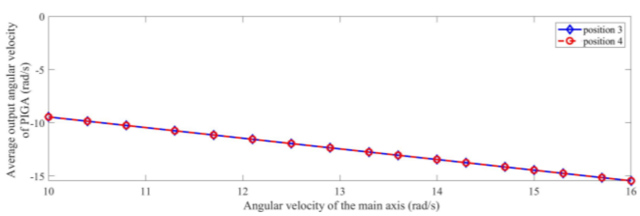

a) average output angular velocity of PIGA.

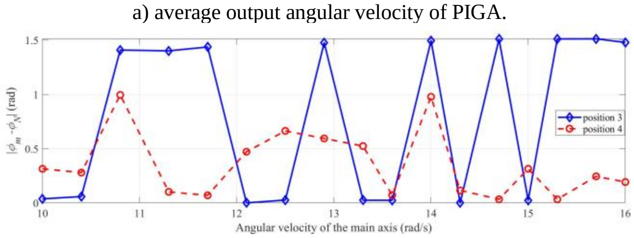

b) angle of the closure error

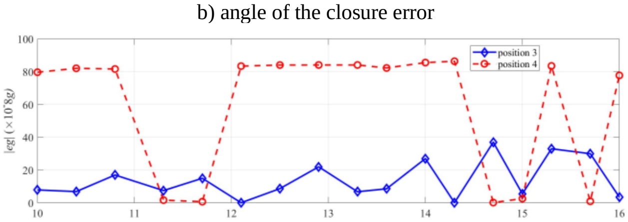

c) error acceleration components caused by closure errors.

Fig.10. Simulation results in positions 3 and 4.

TABLE IV
THE PRECESSION PERIODS OF PIGA IN POSITION 3 AND 4

ω (rad/s)	P_N		ω(rad/s)	P_N	
	Position3	Positio4		Positio3	Positio4
10	86	82	13.6	95	184
10.4	161	139	14	92	214
10.8	89	33	14.3	175	418
11.3	152	117	14.7	174	180
11.7	117	81	15	184	105
12.1	63	79	15.3	188	181
12.5	87	60	15.7	214	213
12.9	107	62	16	190	386
13.3	116	64			

The calibration accuracy r_a (g/g) is given in Fig.9. The calibration accuracy values obtained by the proposed method with parameter optimization are generally lower than the values obtained by the method without parameter optimization. Consequently, the proposed symmetric calibration method can further improve the calibration accuracy of k_{zz}. Moreover, the final calibration accuracy of PIGA could be less than 6×10^{-8} g/g.

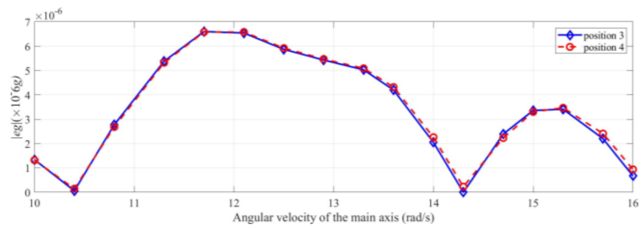

Fig.11. Simulation results of the error acceleration components caused by closure errors in positions 3 and 4 without parameter optimization.

TABLE V
IDENTIFICATION RESULTS OF PIGA IN POSITION 1AND 2

Test method	Identification result(rad/s/g^2)	Calibration uncertainty(rad/s/g^2)	Absolute error(rad/s/g^2)
The proposed method	4.22×10^{-6}	1.29×10^{-6}	7.80×10^{-7}
Test without optimization	7.50×10^{-6}	4.54×10^{-6}	2.50×10^{-6}

The number of the precession periods of PIGA in positions 3 and 4 could be estimated as shown in Table IV. Since the main angular velocity component of PIGA is ω, the average output angular velocity of PIGA is slightly different between position 3 test and position 4 test, as shown in Fig.10.a). Although, the values of $|\phi_m-\phi_N|$ are higher than the ones in positions 1 and 2, the estimation results of $|eg|$ are all lower than 8.5×10^{-7}g as shown in Fig.8.c). Thus, the influence of closure errors on the calibration test can also be ignored.

The simulation results of the $|eg|$ in positions 3 and 4 are shown in Fig.11 for the constant number of the precession period of PIGA equal to 50 (P_N=50). Compared with the simulation results in Fig.10. c), the error acceleration components $|eg|$ are much higher and the maximum value is higher than 6×10^{-6}g. Therefore, it can be concluded that the closure errors have a significant influence on the calibration accuracy of PIGA.

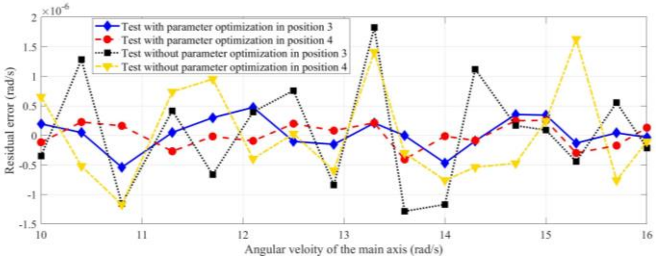

Fig.12. Residual error in positions 3 and 4.

According to Eq. (25), the identification result of k_2', the calibration uncertainty, and the absolute error are calculated as shown in Table V. It is verified that the proposed calibration method with optimizing the test parameter can accurately calibrate k_2' in positions 3 and 4. The calibration uncertainty is decreased from 4.54×10^{-6} rad/s/g^2 to 1.29×10^{-6} rad/s/g^2. Furthermore, the order of magnitude of the absolute error is decreased from 10^{-6} to 10^{-7}. In addition, the residual errors of the two test methods in Fig.12 illustrate that the residual errors are restrained in $\pm 6\times10^{-7}$rad/s by utilizing the proposed calibration test in this paper. In contrast, without parameter optimization, the maximum value of the residual errors is 1.82×10^{-6}rad/s. Thus, the proposed calibration test can significantly improve the calibration accuracy of PIGA.

The simulation results show that the symmetry calibration method of PIGA can effectively avoid misalignment errors and suppress the influence of the closure error on calibrating the nonlinear error coefficients of PIGA. Compared with the method in [24], the magnitude of the calibration uncertainty of k_{zz} is decreased from 10^{-6} to 10^{-7}. However, the symmetric calibration in positions 1 and 2 cannot improve the calibration accuracy of k_3. Moreover, the calibration accuracy of k_{oq} is decreased. Compared with the test without parameter optimization, the calibration uncertainty of k_2' is decreased to approximately one-third of the original value by the proposed calibration method.

VII. Conclusions

In this paper, the symmetric calibration method was proposed to calibrate the nonlinear error parameters of Pendulous Integrating Gyroscopic Accelerometer (PIGA). According to the established corresponding coordinate systems, the precision input accelerations and angular velocities along the three reference axes of PIGA were deduced. Then, to calibrate the main nonlinear error parameters of PIGA, the symmetric calibration model of PIGA on centrifuge testing was established. The axial wobble, axial runout, misalignment errors, and installation errors can be avoided and suppressed by the integer period testing of PIGA precession in the symmetric positions. In addition, since the closure errors were significantly restrained by designing the optimal test parameter and procedure, the measurement accuracy of the calibration test was further improved. Finally, the simulation results were presented to show the effectiveness of the proposed calibration method. Comparison with the calibration test without parameter optimization indicates that the proposed method can significantly reduce the influence of misalignment errors and closure errors. In other words, such calibration tests can improve the calibration accuracy of PIGA. Future work is in progress to address the issues and research challenges of the multi-sensor calibration on a new precision dynamic centrifuge.

References

[1] S. Khankalantary, S. Ranjbaran, and S. Ebadollahi, "Simplification of calibration of low-cost MEMS accelerometer and its temperature compensation without accurate laboratory equipment," *Meas. Sci. Technol.*, vol. 32, no. 4, p. 045102, Feb., 2021.

[2] D. Xu, Y. Chen and R. Kang, "Study of Accelerated Stability Test Method for Quartz Flexible Accelerometer," *IEEE Trans. Device. Mater. Reliab.*, vol. 11, no. 1, pp. 148-156, Mar., 2011.

[3] R.E. Hopkins, F.K. Mueller, and W. Haeussermann, "The pendulous integrating gyroscope accelerometer (PIGA) from the V-2 to trident D5, the strategic instrument of choice," in *AIAA Guidance, Navigation, and Control Conference & Exhibit*, Montreal, Canada, Aug. 2001, pp. 1-9.

[4] P. Gao, K. Li, L. Wang, and Z. Liu, "A Self-Calibration Method for Accelerometer Nonlinearity Errors in Triaxis Rotational Inertial Navigation System," *IEEE Trans. Instrum. Meas.*, vol.66, no.2, pp. 243-253,Feb. 2017.

[5] H. Carlsson, I. Skog and J. Jaldén, "Self-Calibration of Inertial Sensor Arrays," *IEEE Sensors J.*, vol. 21, no. 6, pp. 8451-8463, March, 2021.

[6] P. Gao, K. Li, T. Song and Z. Liu, "An Accelerometers-Size-Effect Self-Calibration Method for Triaxis Rotational Inertial Navigation System," *IEEE Trans. Ind. Electron.*, vol. 65, no. 2, pp. 1655-1664, Feb. 2018.

[7] F. Belkhouche, "A Differential Accelerometer System: Offline Calibration and State Estimation," *IEEE Trans. Instrum. Meas.*, vol. 68, no. 9, pp. 3109-3118, Sept. 2019.

[8] P. Batista, C. Silvestre, P. Oliveira, and B. Cardeira, "Accelerometer Calibration and Dynamic Bias and Gravity Estimation: Analysis, Design, and Experimental Evaluation," *IEEE Trans. Control Syst. Technol.*, vol.19, no.5, pp. 1128-1137, Sep. 2011.

[9] T. Xu, X. Xu, D. Xu and H. Zhao, "A Novel Calibration Method Using Six Positions for MEMS Triaxial Accelerometer," *IEEE Trans. Instrum. Meas.*, vol. 70, pp. 1-11, Sep. 2021.

[10] C. Zhang, M. Dai, W. Luo and X. Pan, "High Precision Tri-Axial Quartz Flexible Accelerometers Resolution Measurement Method Based on Tri-Axial Turntable," *IEEE Access*, vol. 8, pp. 53463-53470, Mar., 2020.

[11] X. Li, *et al.*, "Calibration and Alignment of Tri-Axial Magnetometers for Attitude Determination," *IEEE Sensors J.*, vol.18, no.18, pp. 7399 - 7406, Sep. 2018.

[12] M. Gaitan, I. M. López Bautista, and J. Geist, "Reduction of calibration uncertainty due to mounting of three-axis accelerometers using the intrinsic properties model," *Metrologia*, vol. 58, no. 3, p. 035006, Apr., 2021.

[13] M. Zhang *et al.*, "Cross-Coupling Coefficient Estimation of a Nano-g Accelerometer by Continuous Rotation Modulation on a Tilted Rate Table," in *IEEE Trans. Instrum.Meas.*, vol. 70, pp. 1-12, Apr. 2021.

[14] Q. He, C. Zeng, X. He, X. Xu, and Z. Lin, "Calibrating accelerometers for space-stable inertial navigation systems at system level," *Measurement*, vol. 127, pp. 472-480, Oct., 2018.

[15] IEEE Recommended Practice for Precision Centrifuge Testing of Linear Accelerometers, IEEE Standard 836-2009, 2009.

[16] H. Sohrabi, S. Ebadollahi, "Accuracy enhancement of MEMS accelerometer by determining its nonlinear coefficients using centrifuge test," *Measurement*, Vol.112, pp.29-37, Dec., 2017.

[17] H. Nozato, *et al.*, "A comparison of low-shock and centrifuge calibrations using piezoresistive accelerometers," *Metrologia*, vol.55, no. 1, pp.S13-S22, 2018.

[18] S. Ren, Q. Liu, M. Zeng and C. Wang, "Calibration Method of Accelerometer's High-Order Error Model Coefficients on Precision Centrifuge," *IEEE Trans. Instrum. Meas.*, vol. 69, no. 5, pp. 2277-2286, May 2020.

[19] C. Sun, S. -Q. Ren, M. Zeng, C. -H. Wang and R. Huo, "Sequential Calibration Method of Nonlinear Errors of PIGA on Counter-Rotating Platform Centrifuge," *IEEE Trans. Instrum. Meas.*, vol. 70, pp. 1-11, 2021.

[20] D. S. Gnusarev, E. A. Deputatova, D. M. Kalikhman and A. S. Chibirev, "A method to measure linear output characteristic of a compensation type accelerometer by means of a "non-ideal" centrifuge," *2017 24th Saint Petersburg International Conference on Integrated Navigation Systems (ICINS)*, St. Petersburg, Russia, May, 2017, pp. 1-3.

[21] W. Guan, X. F. Meng, and X. M. Dong, "Testing accelerometer rectification error caused by multidimensional composite inputs with double turntable centrifuge," *Rev. Sci. Instrum.*, vol.85, no.12, pp.125003, Dec., 2014.

[22] Z. Jikun and Z. Rong, "Research and Implement of Turntable Centrifuge Dynamic Radius Test," *2019 IEEE/ASME International Conference on Advanced Intelligent Mechatronics (AIM)*, Hong Kong, China, Jul., 2019, pp. 1445-1450.

[23] Y. Sun, S. Ren and C. Wang, "Calibration method of quartz accelerometer on dynamic centrifuge," *Chin. J. Aeronaut.*, pp. 1-11, Nov. 2021.

[24] C. Sun, S. Ren, and Z. Wang, "Calibration method of accelerometer on precision centrifuge and error analysis," *Journal of Chinese Inertial Technology*, vol.27, no.1, pp.121-128, Feb., 2019.

Chuang Sun was born in Harbin, China in 1989. He received the B.Eng. degree from Harbin Institute of Technology in 2012, the M.Eng. degree from the Civil Aviation University of China in 2015, and the Ph.D.degree from Harbin Institute of Technology in 2020.

He is currently a postdoctoral researcher with the Department of Automation, Tsinghua University, Beijing. His current research interests include the multiscale calibration technology, energy internet and digital twins.

Cao-jun Wei (Senior Member, IEEE) received the bachelor's and master's degrees in control theories and engineering from Tsinghua University, Beijing, China, in 1998 and 1996, respectively, and the Ph.D.degree in computer science from the University of Warwick, Coventry, U.K., in 2001. He is currently a Professor of Beijing National Research Center for Information Science and Technology, Tsinghua University, Beijing, China.

He has authored/coauthored more than 200 papers and cited by international scholars for more than 18 000 times. He has authored or edited eight books. His research interests include distributed computing technologies and energy/power applications. Dr. Cao is a Senior Member of the IEEE Computer Society and a member of the ACM and CCF.

Ru Huo, was born in 1988. She received her B.S. degree from Harbin Engineering University, Heilongjiang, China, in 2011, and the Ph.D. degree from Beijing University of Posts and Telecommunications, Beijing, China. From 2015 to 2016, she studied at the University of British Columbia, Vancouver, Canada.

She is currently a lecturer in Beijing University of Technology. Her current research interests include sensor network and industrial internet.